Controlling Surface Mobility in Interdiffusing Polyelectrolyte Multilayers

Pil J. Yoo,[†] Nicole S. Zacharia,[‡] Junsang Doh,[§] Ki Tae Nam,[‡] Angela M. Belcher,[‡,⊥] and Paula T. Hammond[∥,*]

[†]Department of Chemical Engineering and SKKU Advanced Institute of Nanotechnology (SAINT), Sungkyunkwan University, Suwon 440-746, Republic of Korea, [‡]Department of Materials Science and Engineering, Massachusetts Institute of Technology, Cambridge, Massachusetts 02139, [§]Department of Pathology, University of California at San Francisco, 513 Parnassus Avenue, San Francisco, California 94143, and [⊥]Biological Engineering Division and [∥]Department of Chemical Engineering, Massachusetts Institute of Technology, Cambridge, Massachusetts 02139

ABSTRACT The phenomenon of interdiffusion of polyelectrolytes during electrostatic layer-by-layer assembly has been extensively investigated in the past few years owing to the intriguing scientific questions that it poses and the technological impact of interdiffusion on the promising area of electrostatic assembly processes. In particular, interdiffusion can greatly affect the final morphology and structure of the desired thin films, including the efficacy and function of thin film devices created using these techniques. Although there have been several studies on the mechanism of film growth, little is known about the origin and controlling factors of interdiffusion phenomena. Here, we demonstrate a simple but robust method of observing the process of polyelectrolyte interdiffusion by adsorbing charged viruses onto the surface of polyelectrolyte multilayers. The surface mobility of the underlying polycation enables the close-packing of viruses adsorbed electrostatically to the film so as to achieve a highly packed structure. The ordering of viruses can be controlled by the manipulation of the deposition pH of the underlying polyelectrolyte multilayers, which ultimately controls the thickness of each layer, effective ionic cross-link density of the film, and the surface charge density of the top surface. Characterization of the films assembled at different pH values were carried out to confirm that increased quantities of the mobile polycation LPEI incorporated at higher pH adsorption conditions are responsible for the ordered assembly of viruses. The surface mobility of viruses atop the underlying polyelectrolyte multilayers was determined using fluorescence recovery after photobleaching technique, which leads to estimate of the diffusion coefficient on the order of 0.1 μm^2/sec for FITC-labeled viruses assembled on polyelectrolyte multilayers.

KEYWORDS: interdiffusion · polyelectrolytes · self-assembly · viruses · thin films · surface mobility

Electrostatic layer-by-layer (LbL) assembly has received considerable attention as one of the most versatile and important techniques of molecular self-assembly directed to construct controlled nanoarchitectures *via* manipulation of the molecular interactions.[1,2] This technique is based on the alternating adsorption of materials containing complementary charged groups from aqueous solution to form complexed ultrathin films. The thickness of each adsorbed layer can range from several angstroms to tens of nanometers, depending on the type of adsorbing species and processing conditions such as pH and ionic strength. A wide variety of charged species, including polyelectrolytes,[3] biomolecules,[4,5] carbon nanotubes,[6] or inorganic nanoparticles,[7] can be incorporated into the thin film by this technique. Therefore, it allows the creation of highly tuned, functional thin films with nanometer-level control of film composition and structure. Since the first demonstration by Decher *et al.* in the early 1990s,[8,9] the polyelectrolyte layer-by-layer assembly technique has been extensively investigated for various applications in electrical,[10–13] optical,[14,15] biomedical,[16–19] or membrane devices[20–23] owing to its advantages of relative ease of assembly, environmentally friendly and inexpensive processing, and adaptability to a large number of surfaces.

Along with its vast expansion to engineering and applications areas, mechanistic studies for film growth in LbL assembly have been of great interest in the past few years.[24–27] During LbL self-assembly, polyelectrolytes from solution form electrostatically bound complexes with polyelectrolyte functional groups of opposite charge that are present on the surface, leaving excess charge upon adsorption due to charge overcompensation. Therefore, the surface charge of the outermost layer is altered between the anionic and cationic state, and this charge reversal offers a driving force for sequential build-up in LbL assembly. Since the LbL films are constructed by the formation of ionic cross-links between charged functional groups, neutral groups such as deprotonated amines or protonated carboxylic acids are considered to be "unassociated." Because they are not participating in an ionic bond, such groups are considered to be "available" following assembly for chemistry or the formation of new cross-links if pH changes in the immediate environment should occur.

*Address correspondence to hammond@mit.edu.

Received for review December 6, 2007 and accepted February 12, 2008.

Published online March 1, 2008.
10.1021/nn700404y CCC: $40.75

Generally, the LbL process leads to a linearly growing film structure as exemplified in the case of many strongly charged polyelectrolyte multilayers (PEM) systems.[28,29] Strong charge binding between ion pairs yields an ionically cross-linked network, in which the mobility of polyelectrolytes is significantly limited; such systems, which may consist of strong or weak polyelectrolyte systems, can be used to form stratified heterostructures when the composition is varied in groups of layers during assembly. However, many studies have reported cases of LbL assembly in which the film exhibited a superlinear or exponentially growing characteristic with increasing the number of polyelectrolyte desposition.[30–32] Investigations based on confocal microscopy observations revealed that this phenomenon was attributed to the reversible interdiffusion of at least one of the polyelectrolyte species that constitute the film.[31,33] During the interdiffusion process, excess polyelectrolyte can diffuse into the interior of the film structure and subsequently diffuse out to the film surface in alternate steps depending on the types of charged polyions involved in assembly. Understanding the nature of interdiffusion in multilayer assembly is key to learning how to control the phenomenon, as well as creating a means of harnessing diffusion and exchange behavior in multilayer systems to generate new or interesting multilayer structures. By controlling or blocking interdiffusion within heterostructure thin films, one can enable the creation of compartmentalized heterostructures of interest for electrochemical devices,[27] multiple drug delivery thin films,[26] and other complex structures. On the other hand, the polymer mobility that is gained during the interdiffusion process can be utilized for inducing the macroscopic ordering of biomacromolecules on the top surface of the film. Recently, we presented the spontaneous self-assembly of viruses by employing the interdiffusion of polyelectrolytes, where the dominant binding between polyelectrolytes brought about a preferential exclusion of the supramolecular charged viruses in the *z*-direction owing to their relatively low surface charge density and high steric effect compared to those of polyelectrolytes, which eventually led to a two-dimensional monolayer of viruses on the surface.[34] Furthermore, the biotemplating of genetically engineered viruses enabled the fabrication of well-ordered structures of inorganic nanoparticles or nanowires, which were further developed for a virus-based electrode of a lithium-ion battery.[35] More recently we have shown that, for thicker multilayers of the exponentially growing linear polyethylenimine (LPEI)/poly(acrylic acid) (PAA), the lateral mobility of polyelectrolytes within the LbL multilayer top surface can directly enable the surface ordering of viruses; the spatial control of virus thin films was attainable through a relevant patterning process (see Figure 1).[36] Despite a large interest in the interdiffusion phenomenon, its fundamental driving forces and the kinetics of the process are not yet fully understood.[37,38]

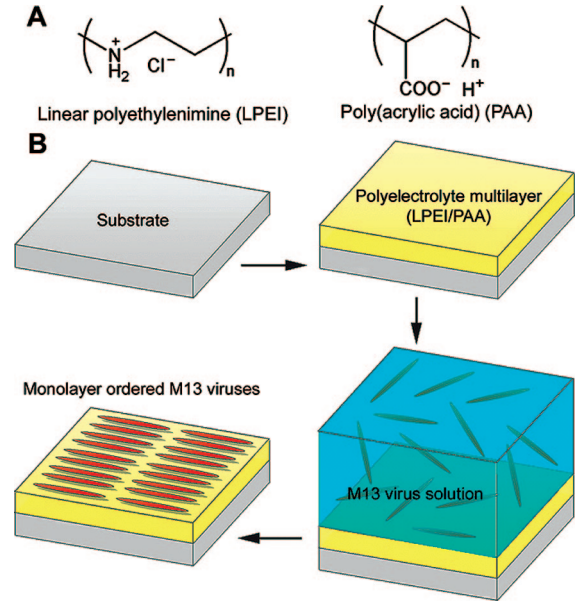

Figure 1. (A) Material structures for layer-by-layer deposition: cationic linear polyethylenimine (left) and anionic poly(acrylic acid) (right). (B) Schematic illustration of experimental procedure for surface mobility induced direct virus assembly on polyelectrolyte multilayer.

The goal of this article is to address these basic questions through direct visualization of the polymeric surface mobility under the conditions amenable to the interdiffusion process. To monitor the diffusional motion of polyelectrolytes on the multilayer surface, we used weakly charged virus molecules as supramolecular probes to reflect the surface motion of the underlying polymeric layer. The lower charge density of the acid-functional virus and its rodlike nature allow it to adsorb electrostatically onto the top flat surface (LPEI) of charged polyelectrolyte multilayers while facilitating its lateral mobility, much as was observed in bulk interdiffusion studies.[34] It was found that variation in the thickness of free diffusing species (LPEI) on the surface could lead to a dramatic change in the lateral mobility of the polyelectrolyte, which was manifest as ordering and assembly behavior of viruses on the top surface.[36] The thickness and composition of the LPEI layers was simply varied by manipulating the pH of film deposition for LBL assembly; films were characterized by spectroscopic and thermogravitric analysis. We also visualized the surface diffusion of the assembled viruses by conducting a fluorescence recovery after photobleaching (FRAP) experiment, and calculated the surface diffusivity of the viruses, which gave a value similar to the reported diffusivity of polyelectrolytes within the multilayers; these findings indicate that the virus mobility is directly tied to the mobility of the underlying polyelectrolyte matrix.

RESULTS AND DISCUSSION

Controlling Virus Assembly on the PEM Surface. In our previous work, we have shown that LPEI is the mobile species in the LPEI/PAA multilayers, which can be utilized for driving a macromolecular self-assembly of viruses.[34] The high mobility of LPEI may be attributed to its relatively low pK_a (100% secondary amines with p$K_a \approx$ 5.5),[39] compared to the higher pK_a of primary amines (p$K_a \approx 9.0-10.0$) in polycations such as poly(allyl amine) or other primary amine containing polymers.[3] The presence of fewer "sticky groups" at intermediate pH that would hinder diffusion of the polymer through the charged multilayer film enables more rapid interdiffusion through the multilayer film. Additionally, the presence of amine groups along the linear backbone of LPEI, particularly in the partially charged state, leads to higher degrees of hydration than the hydrophobic all-hydrocarbon backbones of many synthetic polycations for which amine groups are the side chains. Therefore, the hydrophilic polymer backbone is likely to be more hydrated, and thus more readily plasticized by water molecules; the result is a high polyion chain mobility achieved in the polyelectrolyte multilayer structure.[39,40]

One important advantage of using a weakly charged polyelectrolyte such as LPEI is that its ionic interactions with other charged groups can be readily tuned by the manipulation of assembly pH.[3,41] For example, as the pH is decreased, the degree of ionization will be increased. As a result, its ionic interactions with polyanions in the multilayer film will be enhanced. This increase in ionic interactions may lead to impaired mobility of the polycation. Potentiometric titration of LPEI performed by others revealed that its degree of ionization is increased from 30% to 80% by decreasing the pH value ranging from 8.0 to 3.0 (p$K_a \approx$ 5.5).[42,43] To obtain a stabilized layer-by-layer deposited film, however, charge interactions between LPEI and anionic PAA should also be taken into consideration. In the previous study, stable film growth for LPEI/PAA was achievable in the pH range between 2.5 and 5.5.[39] On the basis of these two criteria, we decided to focus on the pH range between 3 and 5.5 where LPEI exhibits notable changes in the degree of ionization and the structural stability of LPEI/PAA PEM thin film is maintained. Since film deposition at pH 5.5 of LPEI/PAA generates a nonhomogeneous film surface, the upper limit of pH for LBL deposition in this study was further limited to 5.0. This inhomogeneity possibly arises from the weak adsorption, and subsequently easy desorption, of the less charged LPEI from the substrate at high pH conditions relative to the pK_a.

The influence of assembly pH of LPEI/PAA PEM on M13 virus ordering is shown in AFM images of Figure 2. In every case, a pH 4.8 M13 virus solution was applied on 120 nm thickness of LPEI/PAA films that were prepared under different pH conditions from 3.0 to 5.0. The

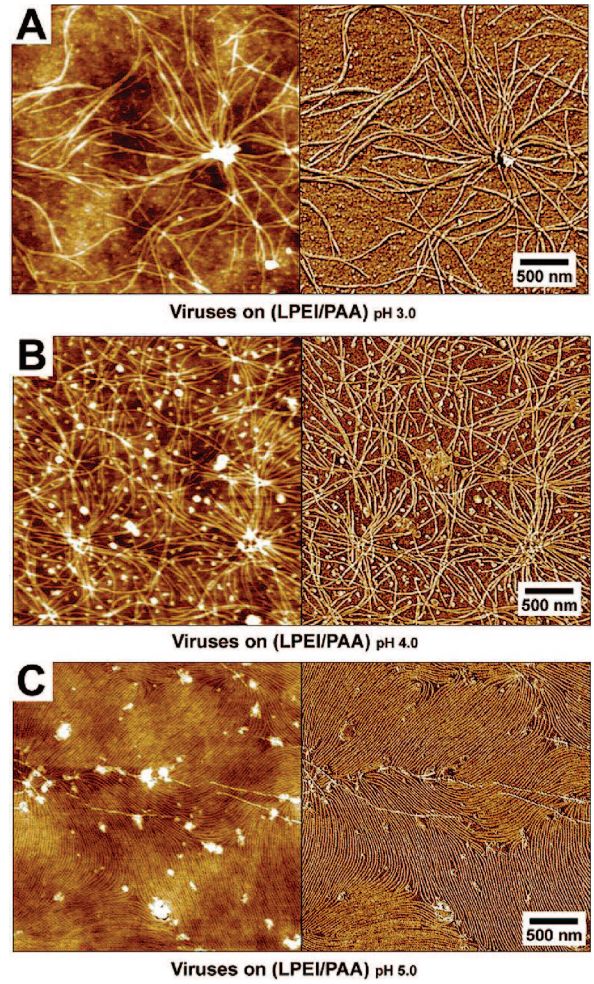

Figure 2. Comparison of different behaviors of virus assembly and ordering depending on deposition pH of underlying polyelectrolyte multilayer films. Atomic force microscopic (AFM) images were captured under dry condition with a scan area of 3 μm × 3 μm. Left-hand side boxes are height mode images (*Z*-range: 20 nm) and right-hand side boxes are phase mode images (*Z*-range: 40°): (A) disordered and aggregated viral assembly on (LPEI/PAA 3.0/3.0)$_{12.5}$; (B) scattered viral assembly on (LPEI/PAA 4.0/4.0)$_{11.5}$ multilayered surface; (C) ordered monolayer assembly of viruses on (LPEI/PAA 5.0/5.0)$_{11.5}$. Ordering density of viruses on the surface is approximately 40 viruses/μm^2.

thickness of 120 nm was chosen because the deposition numbers of LPEI/PAA bilayers grown under different pH conditions coincide at around this thickness, making it possible to use the same numbers of bilayer pairs to gain the desired thickness for each pH condition studied. Notably, very different assembly behaviors of viruses (shown as filamentous wires in AFM images) on the PEM surfaces were observed within this fairly narrow range of underlying PEM deposition pH. The dense ordering of viruses was observed atop the (LPEI/PAA 5.0/5.0)$_{11.5}$ films (Figure 2C), whereas disordered and randomly adsorbed arrangements were observed at lower pH conditions (Figure 2A,B). The viruses adsorb and spontaneously assemble to form a highly ordered phase atop films constructed at pH 5.0 due to the enhanced lateral mobility of the thicker, more weakly

charged layers of LPEI deposited on the multilayer at this pH. The liquid crystalline (LC) nature of the virus[44] can be achieved because of frequent rearrangements on the LPEI/PAA film surface. The interdiffusion behavior of LPEI/PAA during assembly leads to very thick top layers of polyelectrolyte on the multilayer surface once a certain bilayer thickness has been achieved. The top LPEI layer leads to greater mobility of the viruses because there is (a) a decreased effective ionic cross-link density between polymer chain segments in such films, enabling greater overall chain mobility within the film surface layer, and (b) this thicker layer of more weakly associated LPEI chains in the top layer also leads to more swollen, hydrated (*i.e.*, plasticized) films. These two effects result in a surface onto which virus mobility is greatly enhanced, compared to the surfaces of more compact thin films assembled under linear growth conditions. It should also be noted that low surface roughness contributes to the ability of the viruses to assemble into highly ordered monolayer domains on these surfaces. The low roughness on LPEI/PAA films is likely due to the surface annealing effects of the mobile LPEI top layer under hydrated conditions, and improves with increasing pH (decrease in root-mean-square roughness from 1.5 to 0.3 nm with increasing the assembly pH 3 to 5 was obtained for the LPEI topmost layer in LPEI/PAA multilayer films deposited at pH values; see Figure S1 in the Supporting Information). Conventional exponentially growing LbL system is accompanied with prominent surface roughening with increasing numbers of film deposition, making the ability to observe ordering on such systems much more limited. That said, the key parameter to virus mobility and ordering is the mobility of the underlying polymer chains onto which the viruses are electrostatically bound.

The surface mobility of viruses in the ordered phase (Figure 2C) can be temporarily quenched and captured in the dry state for AFM observation. In contrast, the virus assembly $(\text{LPEI/PAA 4.0/4.0})_{11.5}$ indicates a complete lack of ordering. Although the individual electrostatically adsorbed viruses are uniformly distributed on the charged LPEI surface, the reduced surface mobility of LPEI adsorbed as a thinner film at lower pH appears to limit spontaneous LC ordering and packing of viruses. For $(\text{LPEI/PAA 3.0/3.0})_{12.5}$, intriguingly, local aggregations of viruses are expressed as virus bundles observed across the surface. While the major coat proteins of the M13 virus are negatively charged and self-repulsive, the P3 proteins at the terminal end of the virus contain a variety of peptide sequences that are attractive, which leads to end-to-end virus aggregates. Experimental evidence suggests that this aggregation at the end of the viruses takes place in the solution state, not during surface assembly on the polyelectrolyte multilayer. When the top LPEI layer is much thinner and less mobile, as is the case for the multilayers assembled at pH 3.0, these preaggregates do not have an opportunity to rearrange into the more densely ordered arrays seen for LPEI/PAA films assembled at pH 5, for which mobility is greatly increased.

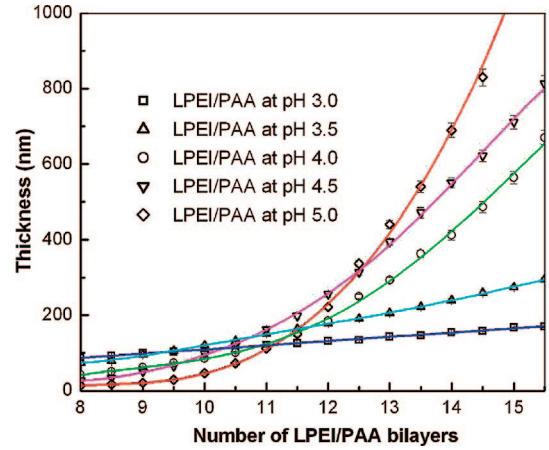

Figure 3. Ellipsometric observations of the film thickness growth with increasing the number of deposition in LPEI/PAA multilayers at different pH condition ranging from 3.0 to 5.0. Films are linearly growing below pH 3.5. Through the transition period at pH 4.0, films are exponentially growing above pH 4.5. Solid lines are linear fit lines or exponentially fit curves depending on growth characteristics. Error bars indicate standard deviations.

Characterization of LPEI/PAA Films. As has been well reported in the literature, the interdiffusion of polyelectrolytes can be found specifically in the superlinearly or exponentially growing films of LbL deposition.[30,31] To elaborate on the relationship between the film deposition pH and interdiffusion—induced surface mobility of LPEI, we checked the thickness growth of LPEI/PAA films by stepwise ellipsometric measurements. As seen from Figure 3, film growth exhibits two different characteristics depending on the pH condition of film deposition: a linear growth profile under pH 3.5 (degree of ionization of LPEI $\approx$ 70% to 80%, pK_a of LPEI $\approx$ 5.5)[42,43,45] and a superlinear (exponential) growth above pH 4.0 (degree of ionization of LPEI $\approx$ 60%). This result provides a crucial hint to the main role of LPEI in a virus ordering on the surface. As the film deposition pH is increased, the LPEI/PAA multilayer film exhibits a more prominent tendency toward exponential growth in thickness, which indicates the enhanced magnitude of LPEI interdiffusion for virus ordering. Under these condition, an increase in the number of bilayer deposition leads to an increasingly thicker layer of top LPEI, with less interpenetration with the underlying polyion layer, and greater mobility of the film at the top surface. At a lower pH condition of film deposition, on the other hand, the highly charged LPEI lacks the ability to interdiffuse, and is kinetically locked to the oppositely charged surface upon adsorption, much as a strongly charged polyelectrolyte renders a linearly growing film. An interesting observation in Figure 3 is that even the exponentially growing films were ultimately exhibiting a linear growth characteristic in the later stages of film

deposition, usually from above 300~400 nm in thickness. Indeed, this transition of exponential to linear growth has been investigated and reported very recently with other interdiffusing polyelectrolyte multilayer systems.[46] Once the film thickness exceeds a certain critical value that corresponds to the limiting distance of polyelectrolyte interdiffusion, then the thickness of diffusion zone is consistently maintained and the film grows in a linear manner, with interdiffusion continuing in the topmost layers of the film.

One question that arises from Figure 3 is a possible relationship between the total thickness of the polymeric multilayer and the ordering behavior of the viruses. To answer this question, we also tested virus adsorption on 200 and 300 nm thick LPEI/PAA films at various pH conditions for LbL deposition. However, no noticeable difference in ordering was observed when compared with the results in Figure 2 (virus assembled on 120 nm thick multilayer of LPEI/PAA). These results, when combined with the fact that ordering occurs only with films greater than around 100 nm, imply that spontaneous ordering of viruses onto the film deposited at the pH 5.0 condition occurs above a certain critical thickness of the underlying PEM. The initial layers adsorbed onto the glass substrate may exhibit conformations greatly influenced by the charged substrate, and initial layers may vary considerably from the higher number layers in composition, particularly in exponentially growing films; thus, a critical thickness implies the existence of a minimum amount of mobile LPEI available at the top surface layer for inducing a viral surface mobility. Above that critical thickness, ordering characteristics are not significantly changed on thicker films (200~300 nm). The experimentally acquired value for the minimum thickness of the multilayers for a highly ordered virus assembly was 90~100 nm, which corresponds well with a previous study.[36]

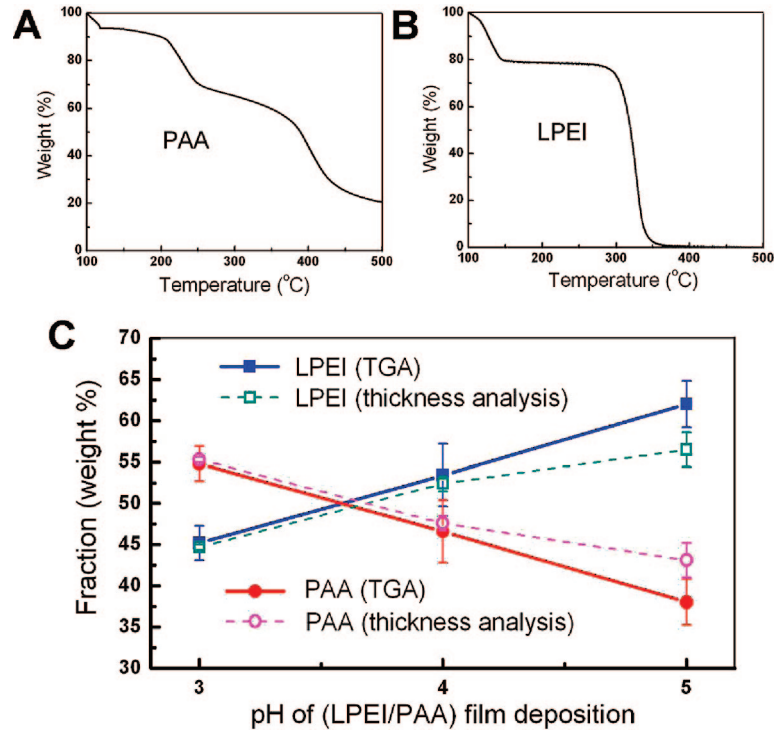

Figure 4. Thermogravimetric analysis of (A) pure PAA and (B) pure LPEI. For films of complexed LPEI/PAA multilayer, specific temperature points of mass decomposition can be determined from the first derivative of decomposition curve, respectively. On the basis of these values, the relative fractions of each component are calculated for multilayered films. (Supporting Information Figure S2). (C) Changes in fractional compositions of LPEI and PAA in LPEI/PAA films; solid lines from TGA analysis and dashed line from thickness analysis of film growth characteristics in Figure.3. As the film deposition pH is increased, the amount of freely diffusional and unassociated LPEI taken by the multilayer film is also increased.

To assess the relative composition between LPEI and PAA in LbL assembled film, we performed thermal gravimetric analysis (TGA) on the dried free-standing films of LPEI/PAA constructed at varying pH conditions. The results of TGA are presented in Figure 4. To evaluate the composition of each species in the multilayered films, we first analyzed PAA and LPEI homopolymer films. Both homopolymers exhibit a slight weight loss between 100 and 150 °C, which corresponds to the desorption of bound water (Figure 4). For PAA, the first thermal decomposition takes place between 175 and 300 °C (Figure 4A), which is attributed to small chains of PAA because of the intrinsically broad polydispersity of the PAA. The second weight loss of high molecular weight PAA begins approximately at 300 °C, and marks the full thermal decomposition of PAA into volatile products. LPEI exhibits a single rapid decomposition above 280 °C after moisture desorption (Figure 4B). Therefore, we can estimate the relative ratio between the LPEI and PAA in polyelectrolyte multilayer films through the analysis of the first derivative of the thermal decomposition curve for multilayered films. The details of the TGA analysis can be found in the Methods section and Supporting Information (see Figure S2). The mass composition of LPEI increases in the films from 45% to 62% with increasing pH within a range of 3.0~5.0 (Figure 5C). The relative fraction of LPEI and PAA in multilayered films was also estimated from the stepwise increase in the film thickness and growth curve data in Figure 3. The increment in thickness for each LPEI or PAA layer was determined from the growth curve, and the cumulative thickness for each polyion was then converted to a mass fraction by considering the density of each homopolymer; the results yield an increase of the LPEI fraction from 45% to 57% with increasing pH within a range of 3.0~5.0.

To obtain further insight on LPEI interdiffusion at the molecular level, we analyzed dry films of LPEI/PAA by FTIR. As shown in FTIR spectra in Figure 5, two slight peaks from the amine functional groups of LPEI are ob-

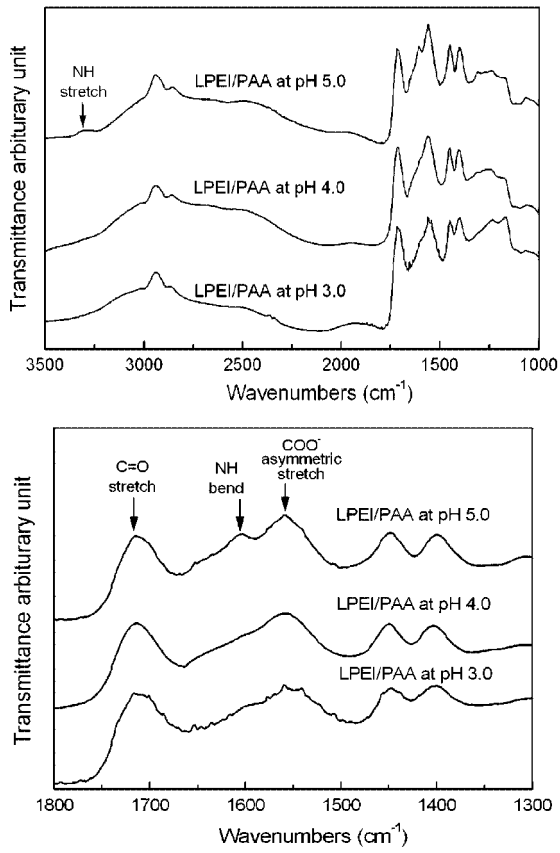

Figure 5. FTIR spectra of LPEI/PAA multilayer assembled at different pH condition ranging from 3.0 to 5.0 (top). The magnified region between 1300~1800 cm^{-1} is presented for a clear identification of peaks (bottom). Spectra are vertically offset for clarity.

served at the pH 5 condition: one at $\nu = \sim 3300\ cm^{-1}$ and another at $\nu = \sim 1610\ cm^{-1}$ that are associated with the N−H stretching and N−H bending bands of the deprotonated secondary amine, respectively. However, the band corresponding to charged amine groups above 3000 cm^{-1} is not readily detectable, because it overlaps nearly entirely with the broad O−H stretching band of the carboxylic acid of PAA. Although the peak intensity of the uncharged amine at pH 5 condition is relatively weak, this result indicates that there are increased amounts of deprotonated LPEI chain segments in the multilayers at this pH than films assembled at lower pHs, providing support to the hypothesis that an increase in the amount of free, unassociated chain segments of LPEI at higher pH conditions can lead to enhanced surface mobility of LPEI.

On the other hand, as shown in Figure 5, two peaks from the carboxylic acid group of PAA are pronounced at all pH conditions: one at $\nu = \sim 1560\ cm^{-1}$ and another at $\nu = \sim 1710\ cm^{-1}$ that indicate the asymmetric stretching band of the ionized carboxylate group and C=O stretching band of the carboxylic acid, respectively. From FTIR data, in general, one can estimate the relative ratio between chemical functions by deconvolution of spectra peaks. By calculating the ratio of the two peaks, an approximation of the percentage of available carboxylic acid groups can be made, by assuming that the absorption coefficient for both groups is approximately the same.[43] We should also account for the amine peaks (1610 cm^{-1}) which also occur in this range, and perform a deconvolution of the peaks between 1500 and 1750, by fitting them with Gaussian peaks, then taking a ratio of the intensities of the peaks at 1560 cm^{-1} (deprotonated COO−) and 1610 cm^{-1} (protonated COOH). On the basis of this idea, we see that the available percentage of carboxylic acid groups in the LPEI/PAA films actually decreases from about 48% at pH 3 to about 41% at pH 5. The details of FTIR analysis can be found in the Supporting Information (see Figure S3).

By considering both the FTIR measurements and the TGA measurements at each of the pH conditions, one can infer the molar quantity of charged acid segments on a given weight basis, and determine the fraction of charged LPEI segments by assuming stoichiometric ionic interactions between charged polyacid and polyamine segments in the multilayer film (details in Supporting Information S3). Using these rough approximations, it is apparent that as assembly goes from pH 3 to pH 5, both the absolute amount of unassociated or free LPEI chain segments in the film as well as the relative percentage of unassociated *versus* ionically bound LPEI segments have increased. This result is indicative of a lowered effective ionic cross-link density, or increased mass of LPEI between ionic cross-links, which results in greater chain mobility for the LPEI segments incorporated into the polyelectrolyte complex network. Through the consideration of the combined TGA and FTIR data and the additional data presented here, we can thus conclude that the increased numbers of unbound, free LPEI chain segments generated at the surfaces of the multilayers formed at higher pH conditions may be responsible for the enhanced surface mobility of LPEI, which ultimately leads to the increased ability of the virus to assemble during adsorption, enabling a spontaneous LC ordered assembly in place of kinetically frozen random arrangements of the virus on the surface.

FRAP Analysis. It is also desired to examine the lateral mobility of adsorbed viruses in the case of spontaneous LC ordering at the surface, to determine whether the lateral mobility of LPEI at the top surface is transferred to the viruses adsorbed atop it. The surface motion of viruses can be monitored *via* attaching fluorescent labels to the virus protein coat. A generalized method for studying the diffusion of surface absorbed molecules is fluorescence recovery after photobleaching (FRAP).[47,48] The procedure involves photobleaching of a locally defined area on a fluorescent sample with a high-intensity laser exposure, generating a sharp contrast in the fluorescence signal. However, surface diffusion of molecules with time yields an intermixing between bleached and nonbleached molecules, which

finally eliminates the difference in fluorescence intensity between them. From this fluorescence recovery characteristic, we can numerically calculate the diffusion coefficient (D) of the adsorbed viruses. Since the first theoretical proposal by Axelrod *et al*. in 1976,[47] FRAP method has been vastly utilized in biological systems, particularly in pharmaceutical research and cell biology. In terms of polyelectrolyte multilayers system, the lateral diffusion of poly(L-lysine)/hyaluronan films, which were also exhibiting superlinear growth profiles characteristic of interdiffusion, was investigated by FRAP experiment and a diffusion coefficient on the order of 10^{-9} cm^2/sec was derived.[49] Another FRAP study of protein diffusion on the surface of a strongly charged traditional PEM film yielded a value of D in the order of 10^{-11} cm^2/sec.[50]

In conventional FRAP analysis, when the bleached beam has a uniform circle profile, recovered fractional fluorescence intensity can be expressed as follows;[47]

$$f_K(t) = \frac{F_K(t) - F_K(0)}{F_K(\infty) - F_K(0)} = 1 - (\tau_D/t)\exp(-2\tau_D/t)[I_0(2\tau_D/t) + I_2(2\tau_D/t)] + 2\sum_{k=0}^{\infty} \frac{(-1)^k(2k+2)!\,(k+1)!\,(\tau_D/t)^{k+2}}{(k!)^2[(k+2)!]^2} \quad (1)$$

where $f_K(t)$ is the fractional fluorescence intensity, $F_K(0)$, $F_K(\infty)$, and $F_K(t)$ are the fluorescence intensity right after bleaching, after infinite time, and after a period of time of t, respectively, τ_D is the characteristic diffusion time, and I_0 and I_2 are the modified Bessel functions.

Figure 6 shows snapshot images of fluorescence recovery of FITC-labeled M13 viruses and its variation in the intensity profile with time. Before photobleaching, viruses are assembled at pH 4.8 onto an LPEI/PAA film surface that was deposited at pH 5.0 conditions, leading to the ordered monolayer structure with an assembly density of approximate 40 viruses/μm^2 (Figure 2C). For fluorescence labeling of the viruses, sequential functionalization of protein coat of the M13 virus was conducted with biotin conjugated anti-fd bacteriophage and FITC conjugated streptavidin. To prevent the nonspecific binding of antibody or fluorescent proteins on the background of the polymeric surface, a small amount of Tween 20 surfactant was added to the solution, leading to a selective binding of antibodies and FITC-streptavidins onto M13 viruses with a minimal background adsorption (see Supporting Information Figure S4). Bleaching with a high power Ar-laser on a circular disk pattern of 40 μm diameter generated a sharp contrast in fluorescence intensity compared with nonbleached backgrounds as shown in Figure 6B. However, PEM interdiffusion, driven by the LPEI species, subsequently generated the enhanced surface mobility of the viruses, and the fluorescence intensity was recovered gradually with time (Figure 6C,D). This technique

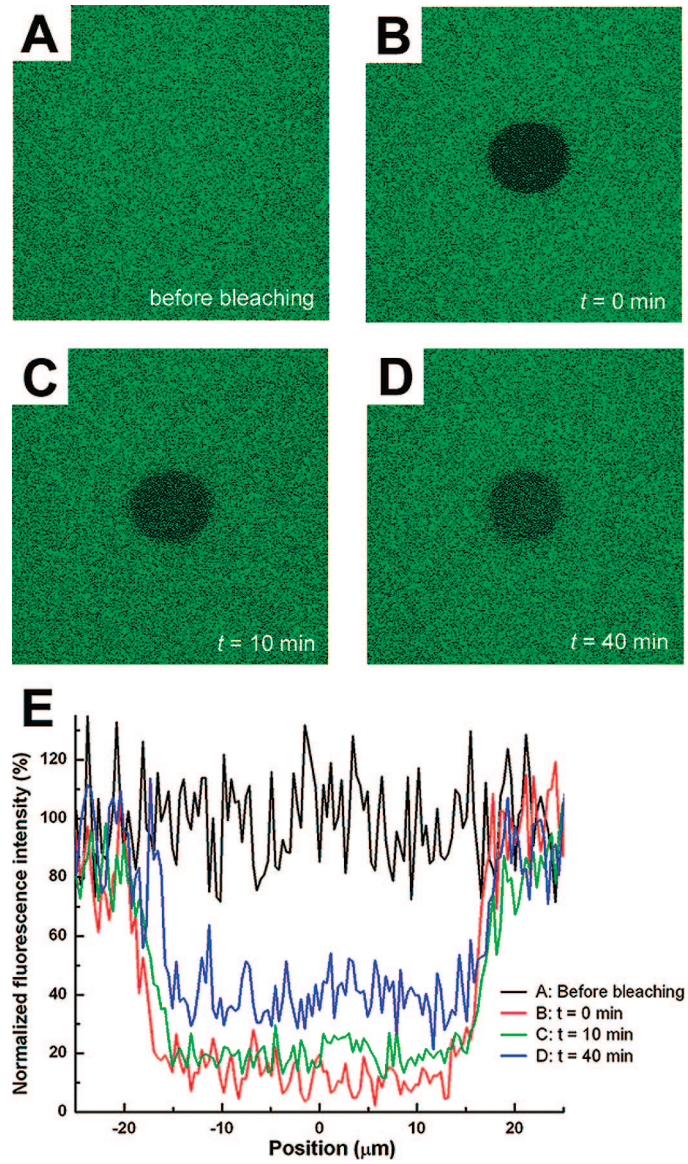

Figure 6. Representative snapshots of FRAP experiment for virus-assembled LPEI/PAA film taken with a confocal laser scanning microscope. Viruses are labeled with FITC-conjugated streptavidin. The diameter of bleached circular area is 40 μm: (A) before photobleaching; (B) right after photobleaching; (C) 10 min after photobleaching; (D) 40 min after photobleaching; and (E) fluorescence intensity profiles corresponding to the images in panels A−D. The intensity profiles are determined from averaging five lines near center of the bleached zone and then relatively normalized with respect to the value of initial fluorescence intensity before photobleaching.

is advantageous in that one can readily visualize the PEM interdiffusion even with a very thin (120 nm) film, as compared to the fact that at least several μm thicknesses of PEM films are required for previously utilized confocal microscopy studies.[30−32] Image profiles in Figure 6E present the quantified values of fluorescence intensities in Figures 6A−D.

Fitting the time-variant fluorescence intensities to the relationship in eq 1 can give the value of the diffusion coefficient of the system. Because of the complexity of the numerical regression of eq 1, however, we used an alternative simplified analysis. It utilizes an-

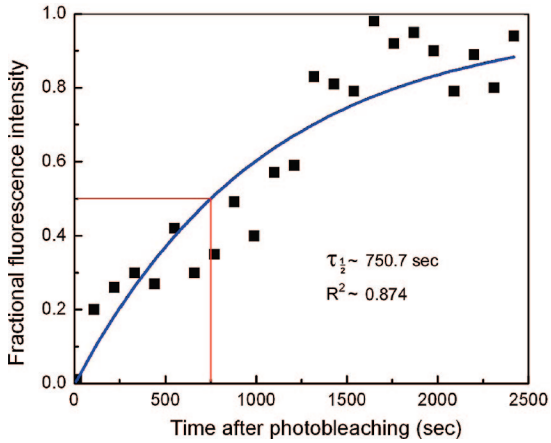

Figure 7. Evolution of the fractional fluorescence recovery as a function of elapsed time after photobleaching for the virus assembled LPEI/PAA multilayer film. Time interval of an image acquisition is 110 s. Solid dots are area-averaged fluorescence intensities for bleached area at each time interval analyzed with the Metamorph program. Blue solid curve represents a fit to the function of exponential decay, from which the characteristic time of $\tau_{1/2}$ can be derived (red line).

other characteristic half-life time $\tau_{1/2}$, which is defined as the time that the fractional fluorescence intensity ($f_K(t)$) reaches 0.5. Considering a modifying factor of γ, which is a constant of shape factor of bleaching beam (for circular beams, γ is 0.88), the diffusion coefficient gives following relation:[47]

$$D = (w^2/4\tau_{1/2})\gamma \qquad (2)$$

As seen from Figure 7, fitting of fractional fluorescence intensity shows a function of exponential decay, in which $\tau_{1/2}$ can be readily determined from the fitted curve. Simple regression procedures for Figure 7 yielded a value of $\tau_{1/2}$ of 750.7 s, which corresponds to a diffusion coefficient D of 0.117 μm^2/sec (1.17×10^{-9} cm^2/sec) for the viruses on the PEM surface, which is very close to the value of the polymeric diffusion coefficient in the interdiffusing poly(L-lysine)/hyaluronan multilayer system ($D \approx 2.2 \times 10^{-9}$ cm^2/sec) that was measured directly from FITC-labeled poly(L-lysine).[49] Considering the bulkiness and ultrahigh molecular weight of the M13 virus (1 μm in length and 14000000 M_w), the resulting diffusion coefficient, which is on the order of 10^{-9} cm^2/sec, is relatively high when compared to the self-diffusion mobility of a typical large charged biomacromolecule such as a DNA molecule (about 10^{-11} cm^2/sec when the molecular weight is on the order of 10^6),[51] which indicates the critical role of thick LPEI layers resulting from exponential growth for enabling the lateral diffusion of viruses. Control experiments with underlying films deposited at pH 3.0 were performed, and little recovery in fluorescence intensity was observed. Under these conditions, the characteristic half-life ($\tau_{1/2}$) was not obtained even after a few hours of fluorescence observation, and therefore a realistic estimate of the corresponding diffusion coefficient not determined. This very slow recovery suggests significantly lower surface diffusion of the viruses atop the pH 3.0 film. It should be noted in this regard that we can observe the lateral motion of LPEI by indirect observation of the surface adsorbed viruses without direct labeling of the LPEI with fluorescent pendant groups that may retard the diffusional motion of linear chains of LPEI. However, there is still an uncertainty in relating the lateral diffusion of viruses with the underlying polyelectrolyte mobility. Surface diffusivity can be underestimated because the idealized surface diffusion should be measured under infinitely dilute adsorption conditions,[52] otherwise the steric repulsions between adsorbed surface molecules can impede diffusion. Therefore, more detailed control experiments are needed to elucidate the interrelationship between viral mobility and the polymeric mobility.

CONCLUSIONS

A new approach for investigating the basis of the interdiffusion phenomena in weakly charged polyelectrolyte multilayers was proposed. To visualize the polymeric interdiffusion process, we induced electrostatic adsorption of M13 viruses onto the charged surface of polyelectrolyte multilayers and utilized the spontaneous ordering of viruses on the LPEI top surface of such multilayers as a means of examining surface mobility on films that enabled virus ordering and packing. When there is interdiffusion of polyelectrolytes into the inner film structure, due to the isotropic characteristic of diffusion to all directions, it accordingly includes the lateral motion of polyelectrolytes on the surface of the film. The lateral mobility of polyelectrolytes can be transferred to surface-adsorbed viruses that have gain the freedom to the spontaneously assemble, leading to the formation of a densely ordered monolayer structure of viruses. When there is no interdiffusion, on the other hand, charged viruses are irreversibly captured on the surface and yield kinetically frozen and randomly assembled structures on the surface.

The interdiffusion of a mobile species of polyelectrolyte can be controlled by altering the pH conditions of layer-by-layer assembly, which affects the numbers of free, nonelectrostatically bound mobile chain segments of polyelectrolyte on the surface. Through the investigation of film thickness with multilayer deposition at different pH conditions, we verified that the exponentially growing films exhibit the interdiffusion of polyelectrolyte. Further investigations from FTIR spectroscopy and thermal gravi-

metric analysis revealed that the surface ordering of viruses was related to the increased composition of the mobile species, LPEI in this case, in the polyelectrolyte multilayers. We also determined the diffusion coefficient of adsorbed viruses from the fluorescence recovery after photobleaching experiment. The lateral motion of fluorescence labeled viruses was observed with confocal laser scanning microscope and a diffusion coefficient of 1.17×10^{-9} cm^2/sec was obtained, which was close to the reported mobility of other interdiffusing polyelectrolytes.

Notably, the ability to control the polymeric interdiffusion with manipulation of film deposition pH offers a potential advantage in certain cases. Because the condition critical to interdiffusion can be directly related to assembly conditions that manipulate the degree of ionization and mobility of the polyion chain, the interdiffusion process can be readily tuned with a single pair of polyelectrolytes. For these situations, the use of a diffusion-blocking layer to prevent interdiffusion between different portions of a composite film, for example, may not be necessary to control the diffusion in the film.[26,53,54] Scientifically, it is anticipated that a deeper investigation of the intriguing surface mobility of supramolecular viruses will also provide a clue to the theoretical analysis of the surface diffusion of highly anisotropic molecules, which has yet to be fully understood.

METHODS

Layer-by-Layer Deposition of Polyelectrolyte Multilayer. Linear polyethylenimine (LPEI, 25000 M_w, monodispersed, Polysciences) and poly(acrylic acid) (PAA, 90000 M_w, polydispersity index (PDI) $\approx$ 4, 25% aqueous solution, Polysciences) were used as-received and prepared as 35 and 20 mM solutions in deionized water, respectively, based on the repeat-unit molecular weight. The molecular structure of LPEI and PAA are presented in Figure 1A. Because of its linear and regular structure, LPEI forms a crystalline solid when unprotonated and is thus insoluble in water above its pK_a. To dissolve LPEI into water, a small amount of HCl solution was added to a mixture of LPEI and deionized water until all the LPEI was dissolved. The pH of both solutions was adjusted to a range from 3.0 to 5.0 carefully with diluted solutions of hydrochloric acid and sodium hydroxide. Silicon substrates were first plasma-treated with a conventional plasma cleaner for 30 s (PDC-001, Harrick Scientific Corp.) to prepare an initial negatively charged surface. Polyelectrolyte multilayers were assembled on prepared silicon substrates by using a HMS programmable slide stainer (Zeiss) with a deposition condition of 15 min adsorption of polyelectrolyte and followed by three sequential washing steps in the bath of deionized water. The nomenclature (LPEI/PAA $m/n)_X$ will be used to denote a multilayer film of X layer pairs of LPEI and PAA deposited at pH m and n, respectively. When X includes 0.5, LPEI is the final adsorbed layer and thus the outermost surface of the multilayer. For the virus assembly atop the LPEI/PAA polyelectrolyte multilayer, 120$\sim$130 nm thickness multilayer films were prepared, which corresponds to 10.5$\sim$12.5 bilayers depending on the pH conditions of film deposition.

Preparation of M13 Virus. The M13 bacteriophage, a virus that only infects bacteria, is composed of $\sim$2700 major coat proteins helically stacked around its single-stranded DNA, rendering a monodispersed and semiflexible filamentous structure (about 1 μm in length and 8 nm in width).[55] Wild-type M13 viruses were amplified using bacterial medium (*Escherichia coli* strain ER2738, New England Biolabs) and diluted in water to the final concentration of $10^9 \sim 10^{10}$ molecules/ml. The solution pH of virus was adjusted to 4.8, near the isoelectric point of M13 virus (see pH$-\zeta$ potential relation of virus in ref 34).

Self-Assembly of M13 Viruses on Polyelectrolyte Multilayer. An experimental schematic for direct assembly of viruses on a PEM surface was shown in Figure 1B.[36] The pH adjusted virus solution was drop-dispensed on a prepared polymer surface for 20$\sim$30 min at ambient temperature. During an adsorption process, negatively charged M13 viruses were electrostatically bound on the positively charged top surface of an LPEI/PAA multilayer. Depending on the multilayer assembly pH, increased interdiffusion ability of LPEI species in polyelectrolyte multilayer structure could further induce the surface reorganization of adsorbed viruses, finally leading to an ordered monolayer structure of M13 viruses on the surface. Virus assembled surfaces were rinsed with deionized water several times to remove loosly bound viruses and dried by nitrogen blowing.

Atomic Force Microscopy (AFM) for Imaging of Virus-Assembled Surface. The surface topology of virus assembled surfaces was characterized with AFM (Digital Instruments, Dimension 3100 with Nanoscope IIIa controller) in dry condition. To minimize any possible misreading during data acquisition and to enhance the image resolution, we used slow scanning tapping mode (0.5$\sim$1.0 Hz of scan speed) with super sharp silicon probes (Pacific Nanotechnology, SSS-NCH, typical tip radius of curvature $\sim$2 nm).

Fourier Transform Infrared Spectroscopy (FTIR) and Thermal Gravimetric Analysis (TGA) for LPEI/PAA Films. FTIR measurements were performed using a Nicolet Magna 860 Fourier transform infrared spectrometer with a DTGS detector. To obtain absorbance spectra, 20 bilayers of LPEI/PAA films were assembled on silicon substrates and measured in transmission mode. For TGA analysis (TA instruments Q50), free-standing films of 100 bialyers of LPEI/PAA were prepared on a neutral surface of Teflon (McMaster Carr Co.) or polypropylene sheet (VWR).[56] Usually, 5 mg of sample was typically used and two runs of TGA were performed for a single film. Three different films made at each pH condition were prepared and therefore averaged values of six runs were used as final data. To minimize moisture and oxygen exposure during TGA experiment, the samples were thoroughly dried in vacuum before testing. Analysis was performed under nitrogen environment. Samples were first heated from room temperature to 120 °C and equilibrated there for 15 min and then ramped further up to 700 °C at a rate of 10 °C/min.

Fluorescence Labeling of M13 Viruses on the LPEI/PAA Multilayers. Biotin conjugated polyclonal rabbit anti-fd bacteriophage antibody (3$\sim$5 μg/ml in water with 0.2 vol. % of Tween 20 detergent, Sigma), which also specifically binds to the M13 virus, was applied onto the assembled virus surfaces for 5 min followed by 1 min of washing with water. Subsequently, a droplet of FITC conjugated streptavidin (1 μg/ml in water with 0.2 vol. % of Tween 20 detergent, Molecular Probes) was applied on the anti-fd bound surface for 5 min to label biotinylated anti-fd bound to M13 viruses. Finally, FITC stained substrates were rinsed with water, and briefly dried under nitrogen. Notably, nonbuffered solutions of antibody and streptavidin were used to exclude any possibility of structural damage or charge rearrangements of an assembled film of polyelectrolyte multilayers and M13 viruses by high ionic strength of buffer solution. We used Tween 20 detergent and a short time period for binding to minimize any nonspecific (*e.g.*, electrostatic or van der Waals interactions) binding of the antibody and streptavidin onto the polyelectrolyte multilayer and substrate. Control experiments were performed with bare films of polyelectrolyte multilayers (without viruses) and successfully confirmed that the fluorescence signal from nonspecific binding was relatively negligible (see Figure S4 in the Supporting Information).

Fluorescence Recovery after Photobleaching (FRAP). FRAP experiments were performed using the confocal microscope (LSM510 METE, Carl Zeiss Microimaging, Inc.) with a 25-mW Ar-ion laser. Fluorescently tagged virus assembled PEM samples were prepared on slide glass and sealed with homemade holders and coverslips to contain the water (500 μl) above the sample surface to prevent sample drying and preserve PEM mobility in the swollen state. The films were photobleached by scanning a defined subregion 100 times with 458 nm, 488 nm, and 514 nm laser lines at maximum laser power. Typically, a 40 μm diameter circular region was used as a bleaching pattern. Subsequently, time-lapse microscopy was performed by acquiring green fluorescence images every 110 s to monitor the fluorescence intensity change upon fluorescent recovery of the bleached area. Collected images were analyzed by Metamorph (Molecular Devices).

Acknowledgment. This work was supported by the Army Research Office in the Institute of Soldier Nanotechnologies at MIT. We also thank Dr. Nicki Watson of the Whitehead Institute for her advising in confocal microscope experiments.

Supporting Information Available: AFM images for surface roughnesses of LPEI/PAA multilayer films assembled at different pH conditions (S1), analysis of TGA data for estimating the relative composition of LPEI and PAA (S2), deconvolution analysis of FTIR data for quantitative estimate the peak intensity and calculations of polyion composition and free and associated functional groups in LPEI/PAA, combining with FTIR and TGA data (S3) and fluorescence and atomic force microscopic images of the selective binding of antibody and proteins on surface ordered M13 viruses (S4). This material is available free of charge *via* the Internet at http://pubs.acs.org.

REFERENCES AND NOTES

1. Decher, G. Fuzzy Nanoassemblies: Toward Layered Polymeric Multicomposites. *Science* **1997**, *277*, 1232–1237.
2. Hammond, P. T. Form and Function in Multilayer Assembly: New Applications at the Nanoscale. *Adv. Mater.* **2004**, *16*, 1271–1293.
3. Shiratori, S. S.; Rubner, M. F. pH-Dependent Thickness Behavior of Sequentially Adsorbed Layers of Weak Polyelectrolytes. *Macromolecules* **2000**, *33*, 4213–4219.
4. Lvov, Y.; Ariga, K.; Ichinose, I.; Kunitake, T. Assembly of Multicomponent Protein Films by Means of Electrostatic Layer-by-Layer Adsorption. *J. Am. Chem. Soc.* **1995**, *117*, 6117–6123.
5. Caruso, F.; Mohwald, H. Protein Multilayer Formation on Colloids through a Stepwise Self-Assembly Technique. *J. Am. Chem. Soc.* **1999**, *121*, 6039–6046.
6. Mamedov, A. A.; Kotov, N. A.; Prato, M.; Guldi, D. M.; Wicksted, J. P.; Hirsch, A. Molecular Design of Strong Single-Wall Carbon Nanotube/Polyelectrolyte Multilayer Composites. *Nat. Mater.* **2002**, *1*, 190–194.
7. Caruso, F.; Lichtenfeld, H.; Giersig, M.; Mohwald, H. Electrostatic Self-Assembly of Silica Nanoparticle—Polyelectrolyte Multilayers on Polystyrene Latex Particles. *J. Am. Chem. Soc.* **1998**, *120*, 8523–8524.
8. Decher, G.; Hong, J. D. Buildup of Ultrathin Multilayer Films by a Self-Assembly Process, II. Consecutive Adsorption of Anionic and Cationic Bipolar Amphiphiles and Polyelectrolytes on Charged Surfaces. *Ber. Bunsen. Phys. Chem.* **1991**, *95*, 1430–1434.
9. Decher, G.; Hong, J. D.; Schmitt, J. Buildup of Ultrathin Multilayer Films by a Self-Assembly Process, III. Consecutively Alternating Adsorption of Anionic and Cationic Polyelectrolytes on Charged Surfaces. *Thin Solid Films* **1992**, *210*, 831–835.
10. Ho, P. K. H.; Kim, J. S.; Burroughes, J. H.; Becker, H.; Li, S. F. Y.; Brown, T. M.; Cacialli, F.; Friend, R. H. Molecular-Scale Interface Engineering for Polymer Light-Emitting Diodes. *Nature* **2000**, *404*, 481–484.
11. DeLongchamp, D.; Hammond, P. T. Layer-by-layer Assembly of PEDOT/Polyaniline Electrochromic Devices. *Adv. Mater.* **2001**, *13*, 1455–1459.
12. DeLongchamp, D. M.; Kastantin, M.; Hammond, P. T. High-Contrast Electrochromism from Layer-by-Layer Polymer Films. *Chem. Mater.* **2003**, *15*, 1575–1586.
13. Eckle, M.; Decher, G. Tuning the Performance of Layer-by-Layer Assembled Organic Light Emitting Diodes by Controlling the Position of Isolating Clay Barrier Sheets. *Nano Lett.* **2001**, *1*, 45–49.
14. Hiller, J.; Mendelsohn, J. D.; Rubner, M. F. Reversibly Erasable Nanoporous Anti-Reflection Coatings from Polyelectrolyte Multilayers. *Nat. Mater.* **2002**, *1*, 59–63.
15. Lee, D.; Rubner, M. F.; Cohen, R. E. All-Nanoparticle Thin-Film Coatings. *Nano Lett.* **2006**, *6*, 2305–2312.
16. Ai, H.; Jones, S. A.; Lvov, Y. M. Biomedical Applications of Electrostatic Layer-by-Layer Nano-Assembly of Polymers, Enzymes, and Nanoparticles. *Cell Biochem. Biophys.* **2003**, *39*, 23–43.
17. Berg, M. C.; Zhai, L.; Cohen, R. E.; Rubner, M. F. Controlled Drug Release from Porous Polyelectrolyte Multilayers. *Biomacromolecules* **2006**, *7*, 357–364.
18. Picart, C.; Schneider, A.; Etienne, O.; Mutterer, J.; Schaaf, P.; Egles, C.; Jessel, N.; Voegel, J. C. Controlled Degradability of Polysaccharide Multilayer Films in Vitro and in Vivo. *Adv. Funct. Mater.* **2005**, *15*, 1771–1780.
19. Fredin, N. J.; Zhang, J. T.; Lynn, D. M. Nanometer-Scale Decomposition of Ultrathin Multilayered Polyelectrolyte Films. *Langmuir* **2007**, *23*, 2273–2276.
20. Farhat, T. R.; Schlenoff, J. B. Ion Transport and Equilibria in Polyelectrolyte Multilayers. *Langmuir* **2001**, *17*, 1184–1192.
21. Xiao, K. P.; Harris, J. J.; Park, A.; Martin, C. M.; Pradeep, V.; Bruening, M. L. Formation of Ultrathin, Defect-Free Membranes by Grafting of Poly(acrylic acid) onto Layered Polyelectrolyte Films. *Langmuir* **2001**, *17*, 8236–8241.
22. Lowman, G. M.; Hammond, P. T. Solid-State Dye-Sensitized Solar Cells Combining a Porous TiO_2 Film and a Layer-by-Layer Composite Electrolyte. *Small* **2005**, *1*, 1070–1073.
23. Lee, D.; Nolte, A. J.; Kunz, A. L.; Rubner, M. F.; Cohen, R. E. pH-Induced Hysteretic Gating of Track-Etched Polycarbonate Membranes: Swelling/Deswelling Behavior of Polyelectrolyte Multilayers in Confined Geometry. *J. Am. Chem. Soc.* **2006**, *128*, 8521–8529.
24. Dubas, S. T.; Schlenoff, J. B. Factors Controlling the Growth of Polyelectrolyte Multilayers. *Macromolecules* **1999**, *32*, 8153–8160.
25. Schlenoff, J. B.; Ly, H.; Li, M. Charge and Mass Balance in Polyelectrolyte Multilayers. *J. Am. Chem. Soc.* **1998**, *120*, 7626–7634.
26. Wood, K. C.; Chuang, H. F.; Batten, R. D.; Lynn, D. M.; Hammond, P. T. Controlling Interlayer Diffusion to Achieve Sustained, Multiagent Delivery from Layer-by-Layer Thin Films. *Proc. Natl. Acad. Sci. U.S.A.* **2006**, *103*, 10207–10212.
27. Zacharia, N. S.; DeLongchamp, D. M.; Modestino, M.; Hammond, P. T. Controlling Diffusion and Exchange in Layer-by-Layer Assemblies. *Macromolecules* **2007**, *40*, 1598–1603.
28. Caruso, F.; Niikura, K.; Furlong, D. N.; Okahata, Y. Ultrathin Multilayer Polyelectrolyte Films on Gold: Construction and Thickness Determination. *Langmuir* **1997**, *13*, 3422–3426.
29. Ladam, G.; Schaad, P.; Voegel, J. C.; Schaaf, P.; Decher, G.; Cuisinier, F. In Situ Determination of the Structural Properties of Initially Deposited Polyelectrolyte Multilayers. *Langmuir* **2000**, *16*, 1249–1255.
30. Lavalle, P.; Gergely, C.; Cuisinier, F. J. G.; Decher, G.; Schaaf, P.; Voegel, J. C.; Picart, C. Comparison of the Structure of Polyelectrolyte Multilayer Films Exhibiting a Linear and an Exponential Growth Regime: An in situ atomic force microscopy study. *Macromolecules* **2002**, *35*, 4458–4465.
31. Picart, C.; Mutterer, J.; Richert, L.; Luo, Y.; Prestwich, G. D.; Schaaf, P.; Voegel, J. C.; Lavalle, P. Molecular Basis for the Explanation of the Exponential Growth of Polyelectrolyte Multilayers. *Proc. Natl. Acad. Sci. U.S.A.* **2002**, *99*, 12531–12535.
32. Lavalle, P.; Picart, C.; Mutterer, J.; Gergely, C.; Reiss, H.; Voegel, J. C.; Senger, B.; Schaaf, P. Modeling the Buildup of Polyelectrolyte Multilayer Films Having Exponential Growth. *J. Phys. Chem. B* **2004**, *108*, 635–648.

33. Lavalle, P.; Vivet, V.; Jessel, N.; Decher, G.; Voegel, J. C.; Mesini, P. J.; Schaaf, P. Direct Evidence for Vertical Diffusion and Exchange Processes of Polyanions and Polycations in Polyelectrolyte Multilayer Films. *Macromolecules* **2004**, *37*, 1159–1162.
34. Yoo, P. J.; Nam, K. T.; Qi, J. F.; Lee, S. K.; Park, J.; Belcher, A. M.; Hammond, P. T. Spontaneous Assembly of Viruses on Multilayered Polymer Surfaces. *Nat. Mater.* **2006**, *5*, 234–240.
35. Nam, K. T.; Kim, D. W.; Yoo, P. J.; Chiang, C. Y.; Meethong, N.; Hammond, P. T.; Chiang, Y. M.; Belcher, A. M. Virus-Enabled Synthesis and Assembly of Nanowires for Lithium Ion Battery Electrodes. *Science* **2006**, *312*, 885–888.
36. Yoo, P. J.; Nam, K. T.; Belcher, A. M.; Hammond, P. T. Solvent Assisted Patterning of Polyelectrolyte Multilayers and Selective Deposition of Virus Assemblies. *Nano Lett.*, in press.
37. Hubsch, E.; Ball, V.; Senger, B.; Decher, G.; Voegel, J. C.; Schaaf, P. Controlling the Growth Regime of Polyelectrolyte Multilayer Films: Changing from Exponential to Linear Growth by Adjusting the Composition of Polyelectrolyte Mixtures. *Langmuir* **2004**, *20*, 1980–1985.
38. Jomaa, H. W.; Schlenoff, J. B. Salt-Induced Polyelectrolyte Interdiffusion in Multilayered Films: A Neutron Reflectivity Study. *Macromolecules* **2005**, *38*, 8473–8480.
39. DeLongchamp, D. M.; Hammond, P. T. Fast Ion Conduction in Layer-by-Layer Polymer Films. *Chem. Mater.* **2003**, *15*, 1165–1173.
40. Clark, S. L.; Hammond, P. T. The Role of Secondary Interactions in Selective Electrostatic Multilayer Deposition. *Langmuir* **2000**, *16*, 10206–10214.
41. Choi, J.; Rubner, M. F. Influence of the Degree of Ionization on Weak Polyelectrolyte Multilayer Assembly. *Macromolecules* **2005**, *38*, 116–124.
42. Smits, R. G.; Koper, G. J. M.; Mandel, M. The Influence of Nearest-Neighbor and Next-Nearest-Neighbor Interactions on the Potentiometric Titration of Linear Poly(Ethylenimine). *J. Phys. Chem.* **1993**, *97*, 5745–5751.
43. Weyts, K. F.; Goethals, E. J. Back Titration of Linear Polyethylenimine—Decrease of pH by Addition of Sodium-Hydroxide. *Macromol. Rapid Commun.* **1989**, *10*, 299–302.
44. Dogic, Z.; Fraden, S. Ordered Phases of Filamentous Viruses. *Curr. Opin. Colloid Interface Sci.* **2006**, *11*, 47–55.
45. Zacharia, N. S.; Modestino, M.; Hammond, P. T. Factors Influencing the Interdiffusion of Weak Polycations in Multilayers. *Macromolecules* **2007**, *26*, 9523–9528.
46. Porcel, C.; Lavalle, P.; Ball, V.; Decher, G.; Senger, B.; Voegel, J. C.; Schaaf, P. From Exponential to Linear Growth in Polyelectrolyte Multilayers. *Langmuir* **2006**, *22*, 4376–4383.
47. Axelrod, D.; Koppel, D. E.; Schlessinger, J.; Elson, E.; Webb, W. W. Mobility Measurement by Analysis of Fluorescence Photobleaching Recovery Kinetics. *Biophys. J.* **1976**, *16*, 1055–1069.
48. Tilton, R. D.; Robertson, C. R.; Gast, A. P. Lateral Diffusion of Bovine Serum-Albumin Adsorbed at the Solid Liquid Interface. *J. Colloid Interface Sci.* **1990**, *137*, 192–203.
49. Picart, C.; Mutterer, J.; Arntz, Y.; Voegel, J. C.; Schaaf, P.; Senger, B. Application of Fluorescence Recovery after Photobleaching to Diffusion of a Polyelectrolyte in a Multilayer Film. *Microsc. Res. Tech.* **2005**, *66*, 43–57.
50. Szyk, L.; Schaaf, P.; Gergely, C.; Voegel, J. C.; Tinland, B. Lateral Mobility of Proteins Adsorbed on or Embedded in Polyelectrolyte Multilayers. *Langmuir* **2001**, *17*, 6248–6253.
51. Maier, B.; Radler, J. O. DNA on Fluid Membranes: A Model Polymer in Two Dimensions. *Macromolecules* **2000**, *33*, 7185–7194.
52. Tilton, R. D.; Gast, A. P.; Robertson, C. R. Surface-Diffusion of Interacting Proteins—Effect of Concentration on the Lateral Mobility of Adsorbed Bovine Serum-Albumin. *Biophys. J.* **1990**, *58*, 1321–1326.
53. Garza, J. M.; Schaaf, P.; Muller, S.; Ball, V.; Stoltz, J. F.; Voegel, J. C.; Lavalle, P. Multicompartment Films Made of Alternate Polyelectrolyte Multilayers of Exponential and Linear Growth. *Langmuir* **2004**, *20*, 7298–7302.
54. Zacharia, N. S.; DeLongchamp, D. M.; Modestino, M.; Hammond, P. T. Controlling Diffusion and Exchange in Layer-by-Layer Assemblies. *Macromolecules* **2007**, *40*, 1598–1603.
55. Flynn, C. E.; Lee, S. W.; Peelle, B. R.; Belcher, A. M. Viruses as Vehicles for Growth, Organization and Assembly of Materials. *Acta Mater.* **2003**, *51*, 5867–5880.
56. Lutkenhaus, J. L.; Hrabak, K. D.; McEnnis, K.; Hammond, P. T. Elastomeric Flexible Free-Standing Hydrogen-Bonded Nanoscale Assemblies. *J. Am. Chem. Soc.* **2005**, *127*, 17228–17234.